Performance Evaluation of Controllable Separate Heat Pipes

Jingyu Cao [a], Jing Li [a], Pinghui Zhao [b], Dongsheng Jiao [a], Pengcheng Li [a], Mingke Hu [a], Gang Pei*, [a]

[a] *Department of Thermal Science and Energy Engineering, University of Science and Technology of China, Hefei 230027, China*

[b] *School of Nuclear Science and Technology, University of Science and Technology of China, Hefei 230027, China*

---

*Corresponding author. Tel.: 0551-63607367. E-mail address: peigang@ustc.edu.cn.

Abstract

A controllable separate heat pipe (CSHP) combined with cool storage can be an efficient and low-cost solution to release the necessary cool power and to improve the precision in the temperature control of cool-storage refrigerators powered by solar energy or electricity with time-of-use price policy. However, the precise temperature control performance of separate heat pipes under active control depends on system design and thus should be confirmed. In this study, a CSHP was developed and an active control method was achieved by interrupting its two-phase natural circulation flow. A one-dimensional steady-state model was used to calculate the critical fill ratio, heat transfer rate, and average working temperature of CSHP. A series of experiments was conducted to analyze the start–stop and heat transfer performances of CSHP at various R134a fill ratios and heat sink temperatures. Under different test conditions, the optimum working points were obtained through fitting. The most suitable control mode was determined and the start–stop performance of CSHP was examined in detail. CSHP starts up quickly in approximately 15 seconds and the quickest stopping time of CSHP approximates to 80 seconds. Therefore, the performance of CSHP under active control can be applied to cool-storage refrigerators.

KEYWORDS: *heat pipe; thermosyphon loop; start-stop; refrigerator; cool storage*

1. Introduction

For energy-saving and environmental considerations, phase-change materials (PCMs) are widely used in many applications. For instance, cool-storage refrigerators provide attractive advantages and promising prospects, especially in the following two fields.

The first field includes photovoltaic (PV) refrigerators. For small cooling capacities in remote areas, a solar PV vapor compression refrigerator is the most viable solar-powered refrigerator [1–3]. In early PV refrigerators, storage batteries are used commonly for long-term operation because of unstable solar energy [4]. Batteries entail huge investments and cause considerable energy wastage in the charge–discharge process. In 2000, Foster et al. designed a battery-free direct drive PV refrigerator and used a water–glycol mixture as a PCM to store cold energy [5]. The cool-storage system stores cold energy on a sunny day and keeps products cold at night without power input. In 2004, Pedersen et al. investigated a solar PV refrigerator without batteries. Pedersen et al. found that the specific cooling capacity of ice is 62% higher than that of lead batteries on the basis of weight [6]. These PV cool-storage refrigerators provide significant advantages in terms of cost and efficiency; thus, solar refrigeration has been highly accepted and distributed.

The second field involves the performance improvement of domestic refrigerators. Power resources have been put to waste and the time-of-use (TOU) price policy has been implemented worldwide because of the significant difference between peak and valley power demand [7]. PCMs have been applied to store cold energy in the valley electric time [8]. As a major energy-consuming home appliance, a cool-storage refrigerator has been considered as promising materials to stabilize electric grids and to reduce electricity bills [9]. This home appliance can also prolong the storage time of fresh food in the event of a power outage. Cool-storage refrigerators are more efficient than traditional direct cooling refrigerators [10].

As a compressor stops working, cool-storage refrigerators cannot precisely control the temperature of fresh food, especially when fresh food compartments are opened frequently. This disadvantage is caused primarily by natural convection between PCM and air in fresh food compartments. In traditional direct cooling refrigerators, the temperature of fresh food compartments is controlled by the start–stop mechanism of compressors. Compressors without frequency conversion functions routinely run for more than 20 minutes within a start–stop cycle to maintain a sufficiently high COP, which directly restricts temperature control performance [11].

A cool-storage system combined with a separate heat pipe can be an efficient and low-cost solution to control the temperature of fresh food in a traditional or cool-storage refrigerator precisely. Figure 1 shows a simplified sample configuration of the novel cool-storage refrigerator. The freezer is located above the fresh food compartment so that the separate heat pipe operates with the assistance of gravity, and the evaporator is located only in the freezer. The compressor of this novel cool-storage refrigerator can operate continuously for hours to store cold energy and the self-acting heat transfer of the separate heat pipe interrupts frequently to control the temperature of the fresh food compartment. Thus, the precision in temperature control and the efficiency of refrigerating systems or PV systems are improved significantly.

Separate heat pipes, which are also named as two-phase thermosyphon loops, wickless gravity-assisted heat pipes, or single-turned pulsating heat pipes, are promising in cool-storage refrigerator applications because of the following characteristics. These pipes can operate passively with the natural circulation of a working fluid, and no additional energy input is needed. These pipes do not comprise moving parts; as such, they are considered simple and reliable. The cost of a separate heat pipe system is low because inexpensive refrigerants, such as water, methanol, and R134a, and common materials, such as copper and aluminum, can be employed. The structure of separate heat pipes can also be changed reasonably to adapt to different applications.

Experimental and theoretical studies on separate heat pipes have been conducted since the 1980s [12]. Chen et al. analyzed the temperature distributions, flow oscillations, overheat phenomenon, and heat transfer coefficient of a double-looped separate heat pipe. Overheat occurs when the liquid charge level is $<35\%$ [13]. Garrity et al. focused on instability observed in a separate heat pipe. Static instabilities are observed in large heat fluxes and are influenced by the height of condensers and by stochastic variations in the flow rate [14]. Franco et al. investigated the heat and mass transfer performances of a small separate heat pipe. The mass flow rate is determined in two different ways to overcome experimental errors and is strongly influenced by the operating pressure and filling ratio [15]. Haider et al. suggested a natural circulation model of a separate heat pipe. Simulations have shown a void fraction variation of 4.0 percent in the evaporator and 2.3 percent in the condenser of the tested entire heat flux range [16].

Separate heat pipes have been used in various practical applications. Khodabandeh et al. suggested a separate heat pipe to cool radio base stations. A heat load of 80 W from a simulated component of less than 1 cm^2 can be dissipated [17].Samba et al. developed a separate heat pipe for cooling telecommunication equipment. The power of telecommunication equipment is increased from 250 to 600 W [18]. Liu et al. investigated a waste heat recovery facility by using a separate heat pipe. Parametric studies have revealed that an increase in the diameter of hydraulics can significantly increase the upper critical values of the initial filling ratio and can slightly extend the lower boundary [19]. Esen et al. investigated a separate heat pipe solar water heater and obtained a 58.96% maximum daily collection efficiency of R410A as a working fluid [20]. Zhu et al. analyzed the application of a separate heat pipe in air-conditioning. In its operation, the average COP is 11.8, and this value is much higher than that of split air-conditioners [21]. Lee et al. proposed the use of separate heat pipes for thermoelectric refrigeration. A heat transfer rate of up to 5400 $W/°Cm^2$ can be obtained [22]. Ling et al. conducted primary performance calculation and investigated a new separate heat pipe refrigerator and a heat pump; Ling et al. found that the use of these devices is feasible [23]. These experimental results have confirmed that separate heat pipes work well under different conditions and that they can be applied to cool-storage refrigerators. Two passive operating modes of separate heat pipes have been widely explored: (1) at imposed temperature, such as solar applications, or (2) at imposed heat flux, such as electronic equipment cooling [24]. However, a relevant ability of separate heat pipe has been neglected; in particular, a precise temperature control capability under active control should be considered.

Precise temperature control is of great importance, and a cool-storage refrigerator combined with separate heat pipe is a new technology. The performance of the precise temperature control of separate heat pipes under active control has yet to be reported within a known range. In this study, a controllable separate heat pipe (CSHP) was developed and the active control method was achieved by artificially interrupting its two-phase natural circulation flow. The performance of CSHP under active control was initially investigated. The factors relevant to its future applications in cool-storage refrigerators were also determined. A one-dimensional steady-state model was used to calculate the critical fill ratio, heat transfer capability, and average working temperature of CSHP. Tests were performed to determine various R134a fill ratios and heat sink temperatures. The heat transfer performance, control mode, and start-stop performance of CSHP were also examined under different experimental conditions. The rapid restarting performance of an incompletely stopped CSHP was also evaluated.

2. Experimental setup

2.1 Operating principle of CSHP

The thermodynamic cycle of CSHP is introduced in Fig. 2. The two-phase natural circulation flow in CSHP can be depicted as follows. First, the liquid working fluid absorbs heat and evaporates in the evaporator. Then, the vapor working fluid flows to the condenser through the vapor line. The working fluid changes from the vapor phase to the liquid phase in the condenser and flows back to the evaporator. The upward movement of the vapor and the downward movement of the liquid occur because of gravity.

The self-acting heat transfer of CSHP can be controlled actively by one or two valves. When the valve is open, the two-phase natural circulation flow transfers heat steadily from the evaporator to the condenser. When the valve is closed, the working fluid stops flowing and the heat transfer capability of CSHP reaches approximately 0. As the two-phase natural circulation flow in CSHP starts and stops quickly, CSHP can operate intermittently to control the heat transfer and the loading temperature.

2.2 Experimental facility description

In Fig. 3, the CSHP experimental facility was designed specifically to develop applications for traditional, cool-storage, and solar PV refrigerators. R134a was chosen as the working fluid because of its low saturation pressure at 5 °C (the common fresh food compartment temperature), environmental protection property, and high stability [25]. Copper was selected as the container material. The condenser is located above the evaporator so that the condensate returns with the assistance of gravity. The vapor line is located between the evaporator outlet and the condenser inlet. The liquid line connects the condenser outlet to the evaporator inlet. The evaporator and the condenser are constituted by the inner tubes of two tube-in-tube helical heat exchangers. A shell inlet and a shell outlet separately exist on the tube-in-tube helical heat exchanger. Valve 1 is located on the upper vapor line and valve 2 is located on the lower liquid line. The particular geometrical parameters of CSHP are listed in Table 1.

Fig. 4 shows the components of the test rig. Performance testing of CSHP was conducted by controlling the evaporator and condenser temperature to provide dependent heat throughput. Two baths were selected to supply water–glycol mixture and water for the heat exchange system as the heat sink and heat source. The evaporator temperature was constant with the help of the water hot bath (DC-0515). The condenser temperature was adjusted by using a water–glycol mixture circulated from the cold bath (DC-3015). The evaporator and condenser heat exchangers were counter flow and spiral type. A heat insulation layer was applied to minimize the cooling loss.

2.3 Measurements

The measurement points of CSHP are shown in Fig. 3. The inlet pressures of evaporator and condenser were measured through two JT-131 pressure sensors of range [0, 16 bars]. The temperature differences of water–glycol mixture and water between the shell inlet and outlet were measured by T-type thermocouples. The wall temperature of vapor and liquid lines were also supervised through many T-type thermocouples. Temperature and pressure measurements were recorded using an Agilent data acquisition instrument with an interval of 5 s. The flow rates of water–glycol mixture and water were measured by two glass rotameters of range [16, 160 L/H]. A vacuum valve and pressure gage were employed to fill and discharge R134a. The mass of R134a filled in CSHP was measured through an electronic scale.

2.4 Experimental procedure

The heat transfer capability of CSHP is represented by the heat transfer capability of evaporator. In addition, a completely stopped CSHP is defined as following conditions: the valve is closed, the water and water–glycol mixture are supplied stably, the heat transfer approximates to zero, and the pressure is constant.

The normal test conditions are adopted when not mentioned in particular and are set as follows: The temperature of water–glycol mixture supplied from cold bath is −25 °C, and the temperature of water flowing from the hot bath is 5 °C. Given the low heat transfer capability of the heat exchange system, the flow rates of water–glycol mixture and water are set as 80L/H and 100L/H, respectively, to maintain an appropriate water temperature difference between the shell inlet and outlet of evaporator (close to 4 °C).

The experiment was performed in following procedure: the R134a fill ratio was verified from 20% to 60% and the inlet temperature of water–glycol mixture was verified from −23 °C to −17 °C. For the normal test condition and its optimal fill ratio, the start–stop performances of three control modes were tested and one was selected for further investigation. Then, the start–stop performance of CSHP was investigated for different experimental conditions. Finally, the quickly restarting performance of CSHP was tested by turning off CSHP from stable operation and then restarting it at a different time before completely stopping.

3. Mathematical models

3.1 Model of critical fill ratio

The start–stop and heat transfer performances of CSHP are affected directly by the working fluid fill ratio. Excessive or insufficient working fluid restricts the performance of CSHP seriously for the following reasons:

(1) If the working fluid is insufficient, the evaporator will be filled with superheated vapor rather than two-phase flow; the evaporator heat resistance will rise sharply.

(2) If the working fluid is excessive, the vapor–liquid mixture will reach condenser through the vapor line and form liquid film in the front part of condenser. Then, condenser heat resistance will rise sharply.

Wang et al. investigated the critical fill ratio model of SHP in 1997 [26]. The critical fill ratios of the separate heat pipe were calculated and validated by experimental results. Yao et al. built a similar calculation model in 2010 [27]. These hypotheses and formulas are adopted in this study:

The fill ratio of R134a in this study is defined as the ratio of volume of liquid R134a and the entire capacity of CSHP:

$$R = \frac{V'}{V} = \frac{m'v'}{V} \tag{1}$$

For a stable operating CSHP, the vast majority of R134a in evaporator and condenser is in a saturated state. The heat insulation layer is sufficiently thick and cooling loss can be ignored. The assumptions for the heat transfer process are as follows:

(1) Only phase-change heat transfer occurs in evaporator and condenser.

(2) Dryness of R134a at the condenser inlet, evaporator outlet, and vapor line is 0.

(3) Steady-flow, steady-state process is assumed throughout the system.

(4) In the evaporator and condenser, the dryness of the R134a changes evenly along the tube.

The R134a in CSHP consists of four parts: the liquid in the liquid line, the vapor in the vapor line and the vapor–liquid mixture in evaporator and condenser.

$$m = m_e + m_c + m_v + m_l \tag{2}$$

where me, mc, mv, and ml are the quantity of working fluid in evaporator, in condenser, in vapor line and in liquid line, respectively.

In the evaporator, the dryness of the working fluid evenly changes along the tube. When the distance away from the evaporator inlet is l, the dryness of R134a can be expressed as:

$$x = \frac{q_m''}{q_m} = \frac{l x_{e,out}}{L_e} \tag{3}$$

On the basis of this equation, we can obtain the quantity of R134a in the evaporator:

$$\begin{aligned} m_e &= \int_0^{L_e} \frac{A_e}{v} dl = \int_0^{x_{e,out}} A_e \left[\frac{1}{xv'' + (1-x)v'} \right] \left(\frac{L_e}{x_{e,out}} \right) dx \\ &= A_e L_e \frac{\ln v' - \ln(v'' x_{e,out} + v' - v' x_{e,out})}{x_{e,out}\left(v' - v''\right)} \end{aligned} \tag{4}$$

where v' is the specific volume of liquid and v'' is the specific volume of vapor.

The quantity of R134a in the condenser can be expressed similarly:

$$m_c = \int_0^{L_c} \frac{A_c}{v} dl = A_c L_c \frac{\ln v' - \ln(v'' x_{e,out} + v' - v' x_{e,out})}{x_{e,out}\left(v' - v''\right)} \tag{5}$$

The dryness of liquid R134a in the liquid line is 0 and the dryness of vapor in the vapor line is xe,out. Their quantity can be expressed as follows:

$$m_v = \frac{A_v L_v}{x_{e,out} v'' + \left(1 - x_{e,out}\right) v'} \tag{6}$$

$$m_l = \frac{A_l L_l}{v'} \tag{7}$$

As the state of R134a at the evaporator outlet is represented by its dryness, xe,out is used to determine the critical fill ratios. Under a lower critical fill ratio, the dryness of R134a at the evaporator outlet is 0. Under an upper critical fill ratio, the entire evaporator is filled with liquid and the dryness of R134a at the evaporator outlet can be regarded as 1. Then, the upper and lower critical fill ratios of CSHP can be calculated. On the basis of the specific geometrical parameters of CSHP in this study, we obtained the calculated upper and lower critical fill ratios of 57% and 30%, respectively.

3.2 Model of heat transfer capability and working temperature

The heat transfer performance of CSHP can be analyzed theoretically via the Ɛ–NTU method [28]. The heat transfer capability of the evaporator is theoretically equal to the heat transfer capability of the condenser. The temperature of R134a in the evaporator and the condenser is constant because of the phase-change heat transfer in these units. The working temperature of CSHP is defined as the constant R134a temperature. The heat transfer capability and working temperature of CSHP can be calculated using the following method:

The heat transfer coefficient of water or water–glycol mixture is expressed by:

$$h = \frac{\lambda N_u}{D} = \frac{\lambda N_u}{D_{sh,i} - D_{tu,o}} \tag{8}$$

where λ is the thermal conductivity of water or water–glycol mixture and N_u is Nusselt's number of water or water–glycol mixture [29].

In the evaporator, $\mathcal{E}_e$ and NTU_e is defined conventionally as follows:

$$NTU_e = \frac{h_e S_e}{\dot{M}_w C_{p,w}} \tag{9}$$

$$\varepsilon_e = 1 - e^{NTU_e} = \frac{t_{w,in} - t_{w,out}}{t_{w,in} - t_e} \tag{10}$$

where $t_{w,in}$, $t_{w,out,}$ and t_e are inlet water temperature, outlet water temperature, and temperature of R134a in evaporator, respectively.

The heat transfer capability in the evaporator is calculated by:

$$\begin{aligned} Q_e &= \dot{M}_w C_{p,w} (t_{w,in} - t_{w,out}) \\ &= \dot{M}_w C_{p,w} \varepsilon_e (t_{w,in} - t_e) \end{aligned} \tag{11}$$

Then, $\dot{M}_w C_{p,w} \varepsilon_{\mathrm{e}} = c_1$:

$$Q_e = c_1(t_{w,in} - t_e) \tag{12}$$

A similar analytical method can be used in the condenser as follows:

$$c_2 = \dot{M}_g C_{p,g} \varepsilon_c \,,\; NTU_c = \frac{h_c S_c}{\dot{M}_g C_{p,g}} \,,\;\; \varepsilon_c = 1 - e^{NTU_c} = \frac{t_{g,out} - t_{g,in}}{t_{g,out} - t_c} \tag{13}$$

where $t_{g,in}$, $t_{g,out}$, and t_c are respectively water–glycol mixture inlet temperature, water–glycol mixture outlet temperature, and temperature of R134a in condenser.

By substituting the initial conditions $t_c = t_e$ and $Q_e = Q_c$ in this analytical model, we can obtain the heat transfer capability and working temperature of CSHP:

$$Q_e = Q_c = \frac{c_1 c_2}{c_1 + c_2}(t_{w,in} - t_{g,in}) \tag{17}$$

$$t_e = t_c = \frac{c_1 t_{w,in} + c_2 t_{g,in}}{c_1 + c_2} \tag{18}$$

According to these equations, the heat transfer capability of CSHP is calculated theoretically. The experimental heat transfer capability of CSHP can be obtained as follows:

$$Q = \rho_w \dot{V}_w Cp_w (t_{w,in} - t_{w,out}) \tag{19}$$

where $\dot{V}_{\mathrm{w}}$ is the measured volume flow rate of water, and $t_{w,in}$ and $t_{w,out}$ are the measured inlet and outlet water temperature of the evaporator, respectively.

4. Results and discussion

4.1 Steady-state working performances

To analyze the steady-state working performances of CSHP, we performed experiments at different fill ratios of R134a. At each fill ratio, $t_{g,in}$ (the inlet water–glycol mixture temperature) was varied from −17 °C to −25 °C. The heat transfer rate in a stable operating state for different R134a fill ratios and $t_{g,in}$, are shown in Fig. 5. Given $t_{g,in}$, the heat transfer rate of CSHP first increases and then decreases with the increment of fill ratio. This variation trend is fitted by a cubic spline interpolation curve. The achieved maximum heat transfer point is defined as the optimal operating point. For rising $t_{g,in}$, the heat transfer capabilities and fill ratios of optimal operating points decrease. The detailed data are recorded in Table 3. For the normal test condition, the maximum heat transfer capability is obtained for a fill ratio of approximately 38.9%. Excessive or insufficient R134a obviously restrict the heat transfer capability of CSHP. For different heat sink temperatures, the fill ratios of optimal working points vary from 34.74 to 38.9%. These optimal fill ratios are reasonable because the calculated values of upper and lower critical fill ratios were respectively 57% and 30%.

The saturation temperature of R134a in the evaporator represents the experimental working temperature of CSHP. The saturation temperature can be obtained by testing the saturation pressure in the evaporator. The variations of working temperatures for various fill ratios and $t_{g,in}$ are shown in Fig. 6. The working temperature increases steadily with the fill ratio and $t_{g,in}$. The heat transfer capabilities and working temperatures of optimal operating points were theoretically calculated by the Ɛ–NTU method. The calculations and the experimental fitting results are compared in Table 3, with relative errors less than 10%.

4.2 Control mode

The active control mode plays a significant role in CSHP. In this test rig, three active control modes exist for the natural two-phase circulation flow control:

(1) Control mode A: The valve located on the upper vapor line is taken as the only switch

(2) Control mode B: The valve located on the lower liquid line is taken as the only switch

(3) Control mode C: Two valves together are taken as switches

Experiments were conducted for the normal test condition and its optimal fill ratio of 38.9% to choose the most suitable control mode for further study. The start-stop performances of control modes A, B, and C were tested; the results were compared. As shown in Fig. 7, time consumed for start-up procedures in three control modes is within 10–15 seconds. In control modes A and C, CSHP takes less than 2 minutes to stop transfer heat, which is obviously quicker than in control mode B. The pressure variations of stopping procedure in control mode A and C are compared in Fig. 8. After

CSHP stops transferring heat, both control modes A and C require more than 200 seconds to achieve a stable stopping state.

Under the novel application background of cool-storage refrigerator, the economic cost of CSHP is a key factor. Considerable investment can seriously restrict the application of products. Compared with control mode A, one additional electronic valve is required in control mode C, which will significantly increase the investment. Therefore, even though the start-stop performance of control mode A is not the best, it is still chosen for further investigation because of cost advantage. The following studies on start-stop performance of CSHP were based on the control mode A.

4.3 Start-up performance

The start-up response of CSHP for different R134a fill ratios in the normal test condition is shown in Fig. 9. The fill ratios are within the range of the calculated critical values. Although the heat transfer capability of the stable operating CSHP varies with fill ratio, the start-up time is approximately 15 seconds. Correspondingly, the pressure variations in evaporator and condenser are shown in Fig. 10. Several phenomena can be observed in the start-up procedure: the heat transfer reaches stability quickly; the pressure difference between evaporator and condenser decreases; the average pressure increases; the difference of average pressure between operating and inactive CSHP becomes larger as R134a fill ratio increases.

In a completely stopped CSHP, liquid R134a is extruded from the evaporator by hot vapor and the liquid level difference is larger. Moreover, the flow of R134a in the working CSHP results in several pressure drops, such as frictional pressure drop, accelerated pressure drop, and local pressure drop. Thus, the pressure difference between evaporator and condenser of a completely stopped CSHP is larger. As long as the valve opens, this large pressure difference will force liquid R134a into the evaporator and then the circulation flow forms quickly in CSHP.

The average pressure obviously varies in the start-up procedure, and is caused by the different R134a distributions between operating and inactive states. In a completely stopped CSHP, the two-phase boundaries are located in the condenser and liquid line; hence, the average pressure is affected primarily by the low condenser temperature. By contrast, in a stable working CSHP, the average pressure is affected simultaneously by the phase-change temperatures in evaporator and condenser.

At the fill ratio of 40%, a transient heat transfer enhancement can be observed. This phenomenon is caused primarily by the following reasons. Compared with the operating state, a completely stopped CSHP has a larger liquid level difference, higher liquid temperature, and larger temperature difference between the heat source and heat sink. When CSHP starts, the flow rate of R134a is enhanced transiently by these factors, and then the heat transfer limit caused by overheating and undercooling is weakened temporarily. Given that the circulation flow stabilizes quickly, the transient heat transfer enhancement disappears in 60 seconds.

These factors are strongly relevant to the difference of average pressure between operating and inactive CSHP. $t_{g,in}$ was varied from −25 °C to −17 °C to change the difference in the average pressure between operating and inactive CSHP. The intension of the transient heat transfer enhancement increases stably with $t_{g,in}$, shown in Fig. 11. Correspondingly, the rising variations of the average pressures for various $t_{g,in}$ are depicted.

The thermal resistance of water in the evaporator was also adjusted by altering the volume flow rate of water to change the difference in the average pressure between operating and inactive CSHP. The intension of the transient heat transfer enhancement is represented by r, which is equal to the percentage of transient heat transfer capability increment. The difference of average pressure between operating and inactive CSHP is defined as ΔP. The correlation between r and ΔP is shown in Fig. 12, which approximates to a linear positive correlation and supports the above analysis of start-up performance.

r and ΔP are calculated by following formulas:

$$r = \frac{Q_{max} - Q_{op}}{Q_{op}} \tag{20}$$

$$\Delta P = P_{op} - P_{st} \tag{21}$$

4.4 Stopping performance

Figures 13 and 14 show the variations of heat transfer capacities and pressures in stopping procedure for various R134a fill ratios. CSHP stops quickly compared with the start–stop cycle of a traditional refrigerator. Additionally, obvious differences can be observed between their heat transfer capability and pressure downtrends. At lower fill ratios, the heat transfer of CSHP stops quickly with rapid pressure drops. At the fill ratio of 50%, the heat transfer of CSHP stops slowly while the pressure rises slightly at first and remains relatively stable for approximately 200 seconds. The stopping performances of CSHP are summarized in Table 4.

The heat transfer rate decreasing time from 100% to 5% is chosen to represent the stopping performance of CSHP, as shown in Table 4. At this moment, the heat transfer of CSHP is nearly stopped and the remainder heat transfer can be ignored. Under normal test conditions, the stopping performance of CSHP is relatively prominent at a fill ratio of 40%.

$t_{g,in}$ was verified from −25 °C to −17 °C at different R134a fill ratios to investigate the key factors relevant to the optimal stopping performance. The stopping times at different fill ratios and $t_{g,in}$ are shown in Fig. 15. Given a fill ratio of 50%, CSHP stops slowly and remains relatively stable for rising $t_{g,in}$. At a fill ratio of 40%, the stopping time of CSHP increases as $t_{g,in}$ decreases. At a fill ratio of 30%, the stopping time of CSHP decreases as $t_{g,in}$ decreases. These results demonstrate that the stopping performance of CSHP is influenced primarily by the R134a fill ratio. Given the heat sink and heat source, CSHP shuts down in approximately 80 seconds under a suitable R134a fill ratio. Excessive or insufficient R134a has a negative effect on the stopping performance of CSHP.

4.5 Rapid restarting performance

Under the application background of refrigerators, CSHP may need to restart rapidly at any time before it completely stops. Under the normal test condition and at an optimal fill ratio of 38.9%, the stopping procedure of CSHP wastes approximately 200 seconds to reach stability. Thus, the quick restarting performance of CSHP needs to be tested.

As shown in Fig. 16, CSHP restarts for different interval times ranging from 20 seconds to 200 seconds. The state of CSHP before completely stopping can be divided into three stages: CSHP still transferring heat; the CSHP stopping heat transfer, and the pressure is not stable; CSHP is in a stable stopping state. The results show that CSHP is able to restart in 10–15 seconds for different interval times. Moreover, the transient heat transfer enhancement appears and increases gradually in the second stage. In the third stage, the transient heat transfer enhancement stays strongest. The results support the analysis of start-up performance.

5. Conclusions

In this study, a test rig was designed and set up to analyze CSHP. To confirm the feasibility of the use of CSHP in cool-storage refrigerators, we investigated its steady-state working performance, control mode, and start–stop performance. A one-dimensional steady-state model was used to calculate the critical fill ratio, heat transfer capability, and working temperature of CSHP. Tests were conducted by varying the R134a fill ratio, control mode, temperature difference between the heat sink and the heat source, thermal resistance of water in the evaporator, and restarting time. The following conclusions can be obtained from our work:

(1) Under the normal test condition, the optimal heat transfer performance of CSHP can be obtained at the fill ratio of 38.9%. At each $t_{g,in}$, the fill ratios of the optimal working points vary from 34.74% to 38.9%. These optimal fill ratios are reasonable because the calculated values of the upper and lower critical fill ratios were 57% and 30%, respectively. The working temperatures and heat transfer rate of operating points are obtained through calculation and fitting, with relative errors of less than 10%.

(2) The time consumed for the start-up procedures in the three control modes is within 10–15

seconds. In control modes A and C, CSHP requires less than 2 minutes to stop heat transfer. Control modes A and C occur more rapidly than control mode B does. Control mode A is chosen for further analysis because of the cost advantage.

(3) The start-up time of CSHP is approximately 15 seconds at different fill ratios under the normal test conditions. At a fill ratio of 40%, the intensity of transient heat transfer enhancement increases as $t_{g,in}$ decreases. The results of the start-up performance analysis are supported by the approximately linear positive correlation between r_t and ΔP.

(4) The stopping performance of CSHP varies with fill ratio and $t_{g,in}$. The results demonstrate that the stopping performance of CSHP is influenced primarily by the R134a fill ratio. Given the heat sink and the heat source, CSHP shuts down in approximately 80 seconds at a suitable R134a fill ratio. Excessive or insufficient R134a negatively affects the stopping performance of CSHP.

(5) CSHP can restart in 10–15 seconds at any time before it completely stops. The transient heat transfer enhancement significantly differs among the three restarting stages. The results support the analysis results of the start-up performance.

These conclusions indicate that the performance of CSHP under active control is beneficial for its future application in cool-storage refrigerators. Different control methods and working fluids will be investigated in our future work.

Acknowledgments

The study was sponsored by (1) the National Science Foundation of China (NSFC 51476159, 51178442, 51206154, and 51408578), (2) the Fundamental Research Funds for the Central Universities, and (3) Dongguan Innovative Research Team Program (No. 2014607101008).

Nomenclature

A	heat exchange surface [m^2]
C_p	specific heat capacity [$J\ kg^{-1}\ K^{-1}$]
D	diameter [m^2]

h	heat transfer coefficient [W m^{-2} K^{-1}]
L	length [m]
l	distance away from the evaporator inlet [m]
$\dot{M}$	mass flow rate [kg s^{-1}]
m	quantity [kg]
N_u	Nusselt number
NTU	number of transfer unit
ΔP	difference of average pressure between operating and inactive CSHP [MPa]
P	average pressure [MPa]
Q	heat transfer rate [kW]
q	flow rate of R134a [kg s^{-1}]
R	fill ratio
r	percentage of transient heat transfer capability increment
S	cross-sectional area [m^2]
t	temperature [°C]
V	entire capacity of CSHP [m^3]
$\dot{V}$	volume flow rate [m^3 s^{-1}]
v	specific volume [m^3 kg^{-1}]
x	dryness

Greek letters

ε	effectiveness
λ	thermal conductivity [W m^{-1} k^{-1}]
ρ	density [kg m^{-3}]

Superscripts

'	liquid

$''$ vapor

Subscripts

c	condenser
e	evaporator
g	water–glycol mixture
i	inside
in	inlet
l	liquid line
m	mass
max	maximum
o	outside
op	stable operating CSHP
out	outlet
v	vapor line
w	water
sh	shell of tube-in-tube helical heat exchanger
st	completely stopped CSHP
tu	inner tube of tube-in-tube helical heat exchanger

References

[1] Kattakayam, T. A., Srinivasan, K., Thermal performance characterization of a photovoltaic driven domestic refrigerator, International Journal of Refrigeration, 23(2000) 190-196.

[2] Kaplanis, S., Papanastasiou, N., The study and performance of a modified conventional refrigerator to serve as a PV powered one, Renewable energy 31(2006) 771-780.

[3] Anish Modi, Anirban Chaudhuri, Performance analysis of a solar photovoltaic operated domestic refrigerator, Applied Energy 86 (2009) 2583–2591.

[4] Kattakayam, T. A., Srinivasan, K., Lead acid batteries in solar refrigeration systems, Renewable energy 29 (2004) 1243-1250.

[5] R.E. Foster, D. Bergeron, Photovoltaic Direct Drive Refrigerator with Ice Storage: Preliminary Monitoring Results, in: ISES 2001 Solar World Congress, 2001, pp.509-516.

[6] Pedersen, P. H., Poulsen, S., Katic, I., SolarChill-a solar PV refrigerator without battery, In: EuroSun 2004 Conference, 2004, pp. 20-24.

[7] M. H. Albadi, Demand Response in Electricity Markets: An Overview, in: IEEE Power Engineering Society General Meeting, 2007, pp. 1-5.

[8] Guiyin Fang, Xu Liu, and Shuangmao Wu, Experimental investigation on performance of ice storage air-conditioning system with separate heat pipe, Experimental Thermal and Fluid Science 33 (2009) 1149-1155.

[9] Leilei Wang, Jia Yan, et al, Experimental study on cold accumulation and release of peak load shifting refrigerator, Journal of Refrigeration, PR China 29 (2008) 38-41.

[10] Azzouz, K., Leducq, D., Gobin, D., Performance enhancement of a household refrigerator by addition of latent heat storage, International Journal of Refrigeration 31 (2008) 892-901.

[11] P. J. Rubas and C. W. Bullard, Factors contributing to refrigerator cycling losses, International Journal of Refrigeration 94 (1995) 168-176.

[12] Amir Faghri, Heat Pipe Science and Technology, Global Digital Press, Washington, 1995, p. 9.

[13] K. S. Chen, S. T. Tsai and Y. W. Yang, Heat transfer performance of a double-loop separate-type heat pipe Measurement results, Energy Convers. 35 (1994) 1131-114.

[14] Garrity, P.T., Klausner, J.F., Mei, R., Instability phenomena in a two-phase microchannel thermosyphon, International Journal of Heat Mass Transfer 52 (2009) 1701-1708.

[15] Alessandro Franco and Sauro Filippeschi, Experimental analysis of Closed Loop Two-phase Thermosyphon (CLTPT) for energy systems, Experimental Thermal and Fluid Science 51 (2013) 302-311.

[16] Haider, S.I., Joshi, Y.K., Nakayama, W., A natural circulation model of the closed loop two-phase thermosyphon for electronics cooling, Journal of Heat Transfer 124 (2002) 881-890.

[17] Khodabandeh, Rahmatollah, Thermal performance of a closed advanced two-phase thermosyphon loop for cooling of radio base stations at different operating conditions, Applied Thermal Engineering 24 (2004) 2643-2655.

[18] Ahmadou Samba, Hasna Louahlia-Gualous, et al, Two-phase thermosyphon loop for cooling outdoor telecommunication equipments, Applied Thermal Engineering 50 (2013) 1351-1360.

[19] Di Liu, G. F. Tang, F. Y. Zhao, et al, Modeling and experimental investigation of looped separate heat pipe as waste heat recovery facility, Applied Thermal Engineering, 26 (2006) 2433-2441.

[20] M. Esen, H. Esen, Experimental investigation of a two-phase closed thermosyphon solar water heater, Solar Energy 79 (2005) 459-468.

[21] Dan-dan Zhu, Da Yan, Zhen Li, Modelling and applications of annual energy-using simulation module of separate-type heat pipe heat exchanger, Energy and Buildings, 57 (2013) 26-33.

[22] J.S. Lee, S.H. Rhi, C.N. Kim, Y. Lee, Use of two-phase loop thermosyphons for thermoelectric refrigeration: experiment and analysis, Applied Thermal Engineering 23 (2003) 1167-1176.

[23] Z. Ling, et al, A study on the new separate heat pipe refrigerator and heat pump, Applied Thermal Engineering 24 (2004) 2737-2745.

[24] Alessandro Franco and Sauro Filippeschi, Closed Loop Two Phase Thermosyphon of Small Dimensions: a Review of the Experimental Results, Microgravity Sci. Technol. 24 (2012) 165-179.

[25] Tae Woo Lim and Jun Hyo Kim, An Experimental Investigation of Heat Transfer in Forced Convective Boiling of R134a, R123 and R134a/R123 in a Horizontal Tube, KSME International Journal 18 (2004) 513-525.

[26] Wen Wang, Rui Xiong, Chuan-jing Tu, et al, Analysis of the Fill Quantity for Separated Type Heat Pipe, Power Engineering, PR China 17(1997) 66-68.

[27] Yuan Yao, Design and experimental investigation of heat transferring capacity of gravitational separate type which applied to air-condition (M.S. Thesis) South China University of Technology, PR China, 2010.

[28] F. P. lncropera, et al, Fundamentals of Heat and Mass Transfer, John Wiley & Sons, 2011, pp.420-427.

[29] S. Garimella, D. E. Richards, R. N. Christensen, et al, Experimental Investigation of Heat Transfer in Coiled Annular Duets, Journal of Heat Transfer 110 (1988) 329-336.

Figure Captions

Fig. 1. A simplified sample configuration of the novel cool-storage refrigerator.

Fig. 2. An operating CSHP.

Fig. 3. Concrete structure and measurement points of CSHP.

Fig. 4. Concrete structure and components of the test rig.

Fig. 5. Heat transfer rate for different $t_{g,in}$ versus fill ratio.

Fig. 6. Working temperatures for different $t_{g,in}$ versus fill ratio.

Fig. 7. Start-stop performance comparison of three control modes.

Fig. 8. Pressure variations of control mode A and C in the stopping procedure.

Fig. 9. Heat transfer rates for different fill ratios versus time in the start-up procedure.

Fig. 10. Pressures for different fill ratios in evaporator versus time in the start-up procedure.

Fig. 11. Average pressures and heat transfer rates for different $t_{g,in}$ versus time in the start-up procedure.

Fig. 12. r versus ΔP.

Fig. 13. Heat transfer rates for different fill ratios versus time in the stopping procedure.

Fig. 14. Pressures for different fill ratios versus time in the stopping procedure.

Fig. 15. Variations in stopping time with fill ratio and $t_{g,in}$.

Fig. 16. Rapid restarting performance versus interval time.

Table captions

Table 1. Geometrical parameters for CSHP.

Table 2. List of experimental testing and monitoring devices.

Table 3. Comparisons of the calculations and experimental fitting results.

Table 4. Comparisons of the stopping time for different fill ratios.

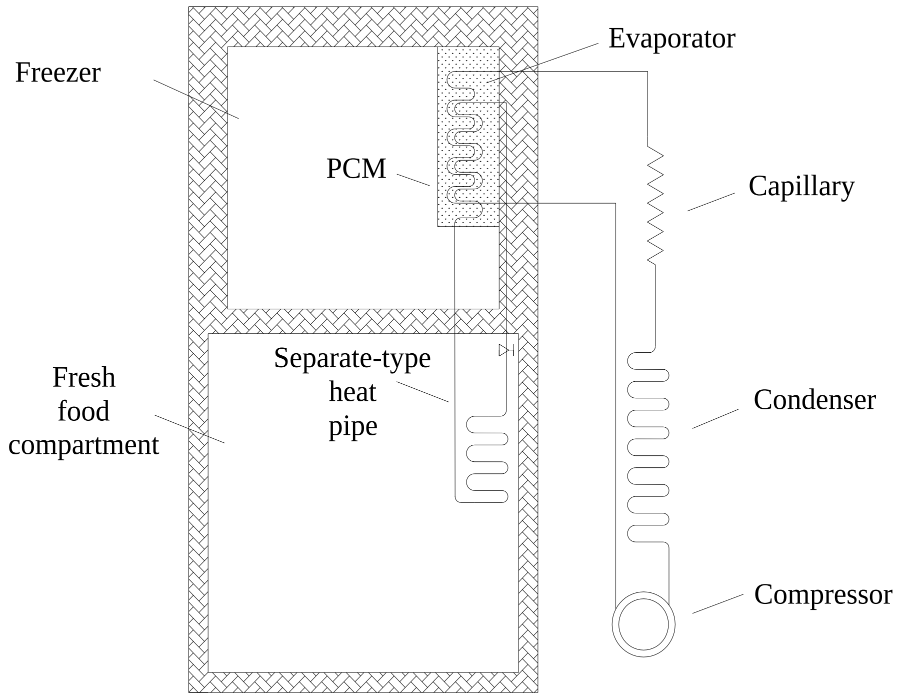

Fig. 1. A simplified sample configuration of the novel cool-storage refrigerator.

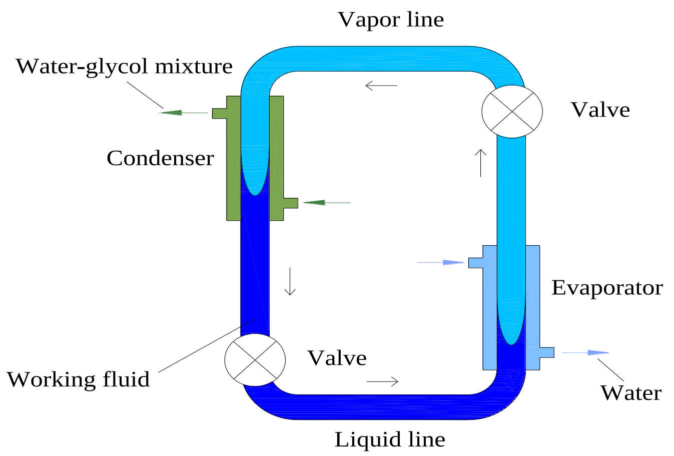

Fig. 2. An operating CSHP.

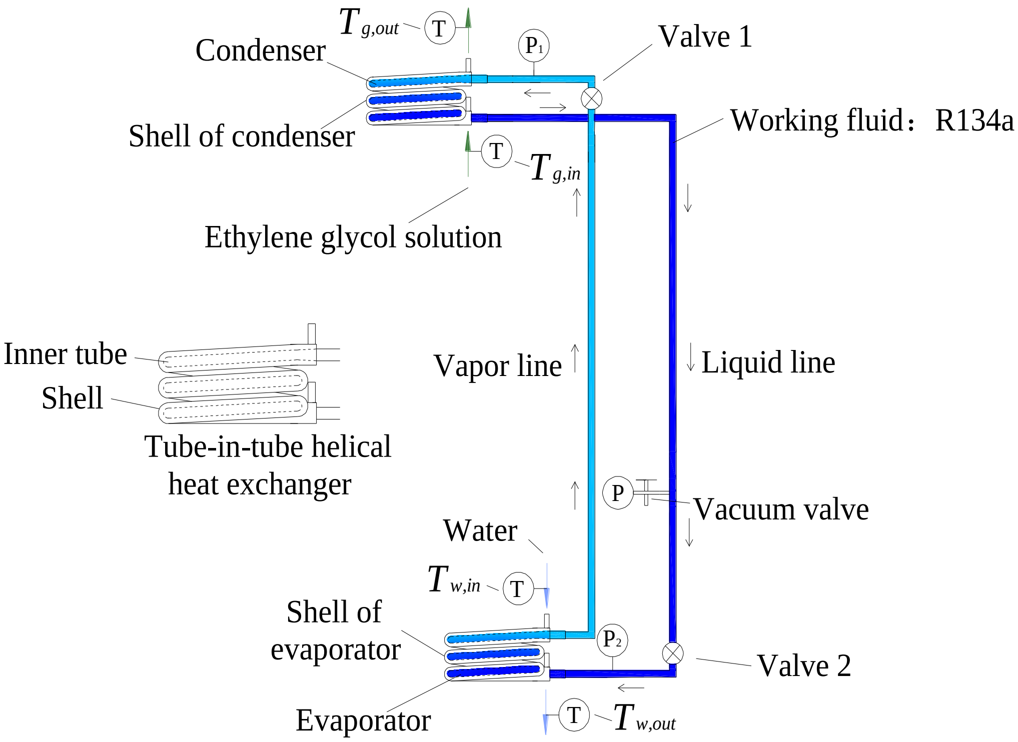

Fig. 3. Concrete structure and measurement points of CSHP.

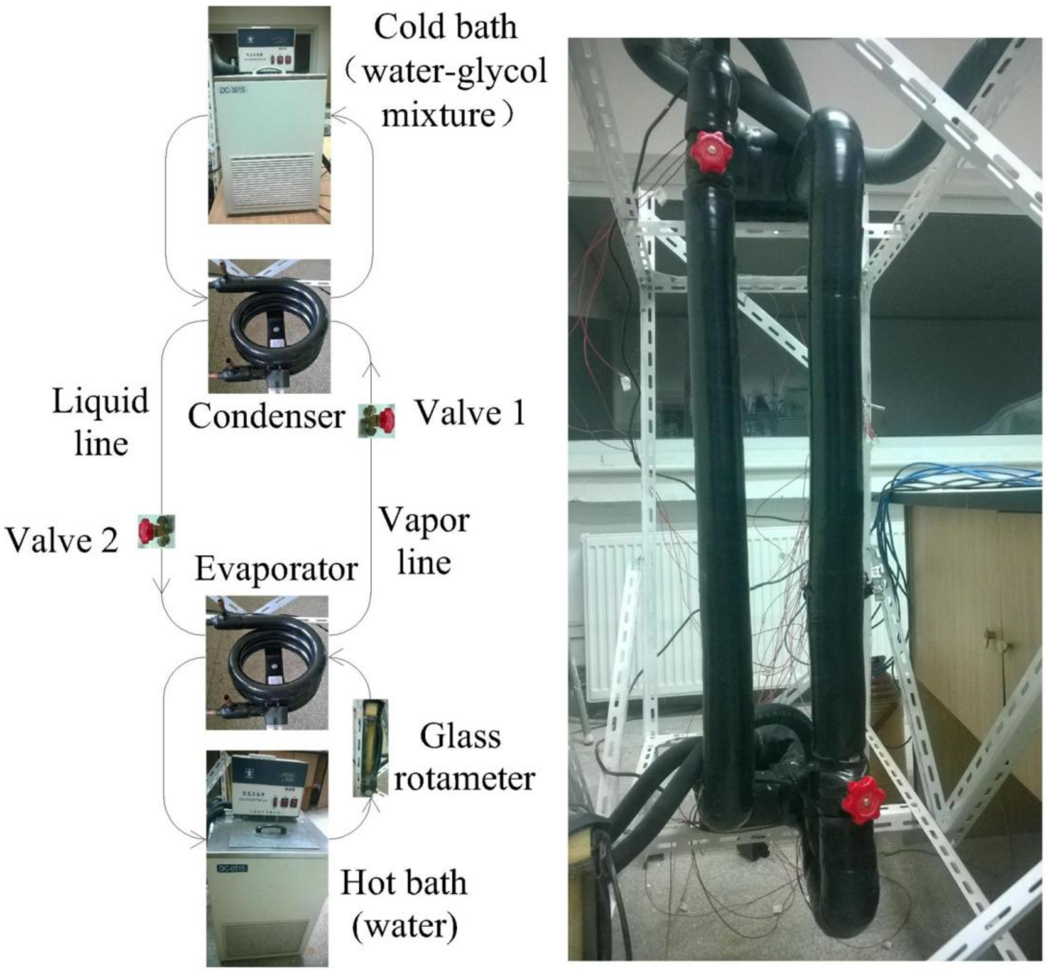

Fig. 4. Concrete structure and components of the test rig.

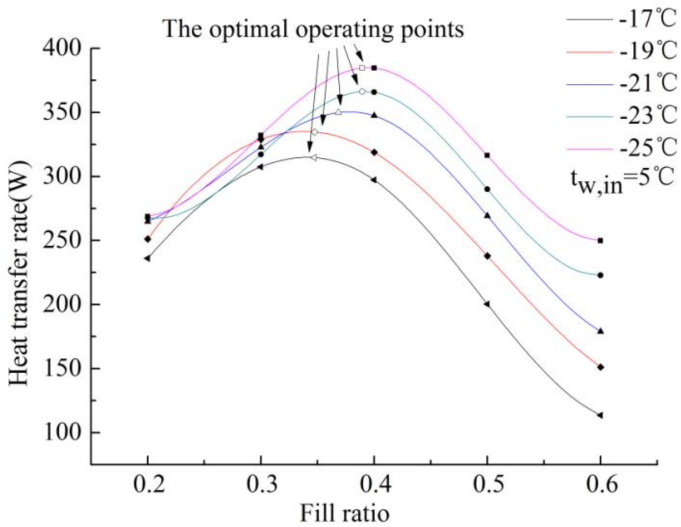

Fig. 5. Heat transfer rate for different $t_{g,in}$ versus fill ratio.

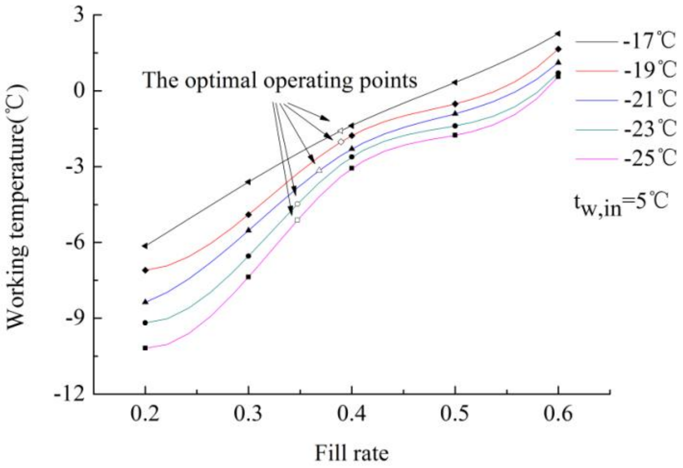

Fig. 6. Working temperatures for different $t_{g,in}$ versus fill ratio.

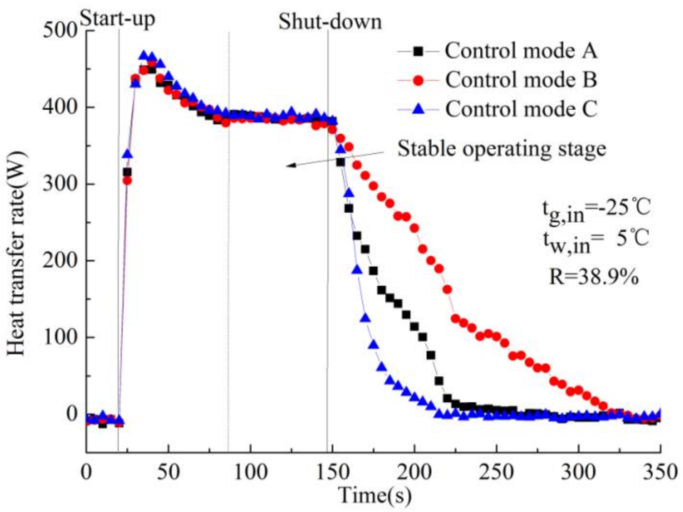

Fig. 7. Start-stop performance comparison of three control modes.

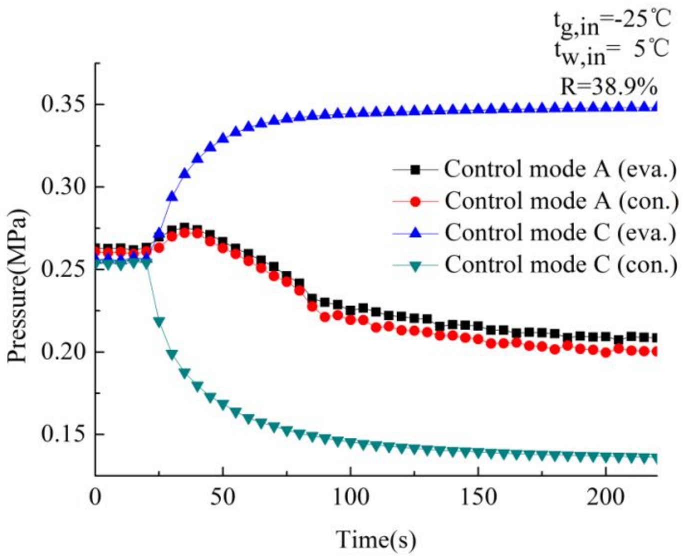

Fig. 8. Pressure variations of control mode A and C in the stopping procedure.

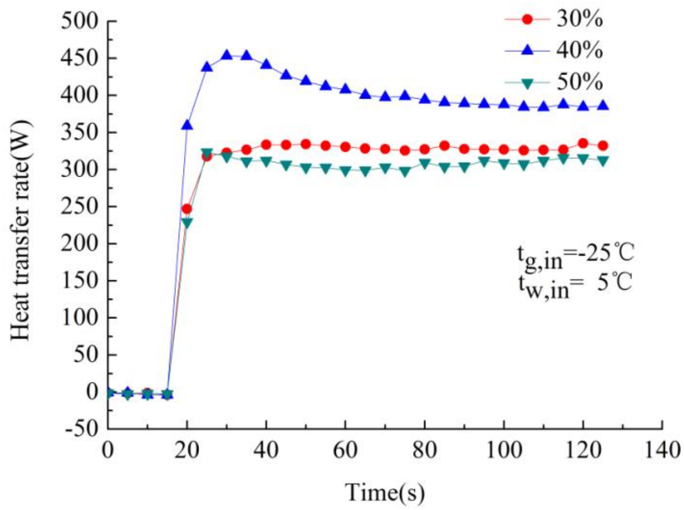

Fig. 9. Heat transfer rates for different fill ratios versus time in the start-up procedure.

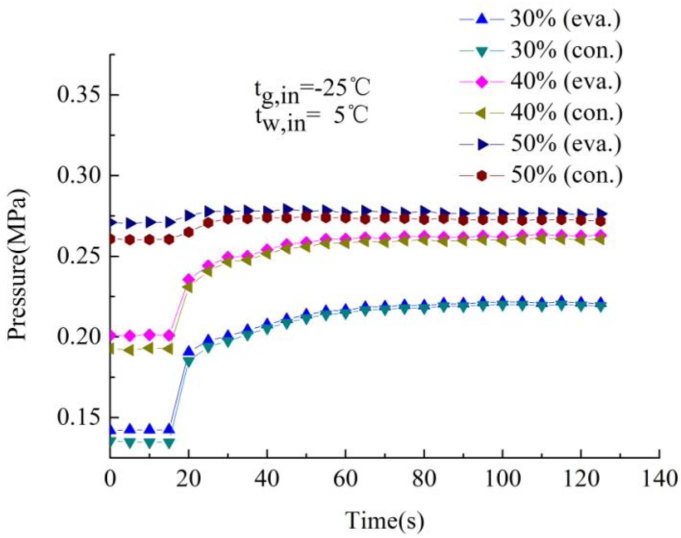

Fig. 10. Pressures for different fill ratios in evaporator versus time in the start-up procedure.

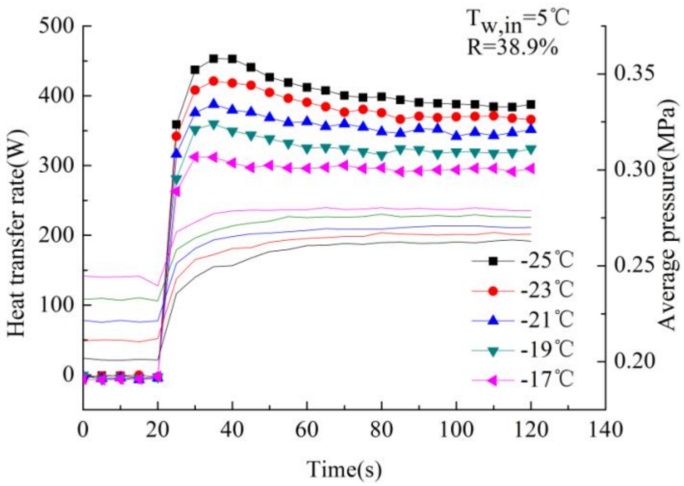

Fig. 11. Average pressures and heat transfer rates for different $t_{g,in}$ versus time in the start-up procedure.

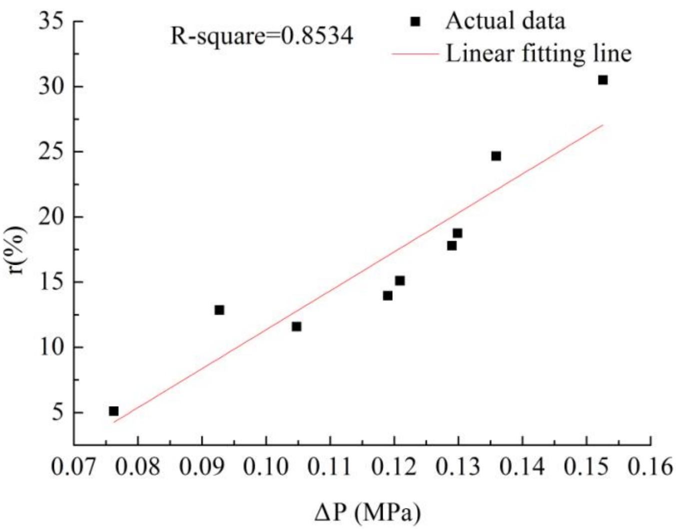

Fig. 12. *r* versus *ΔP*.

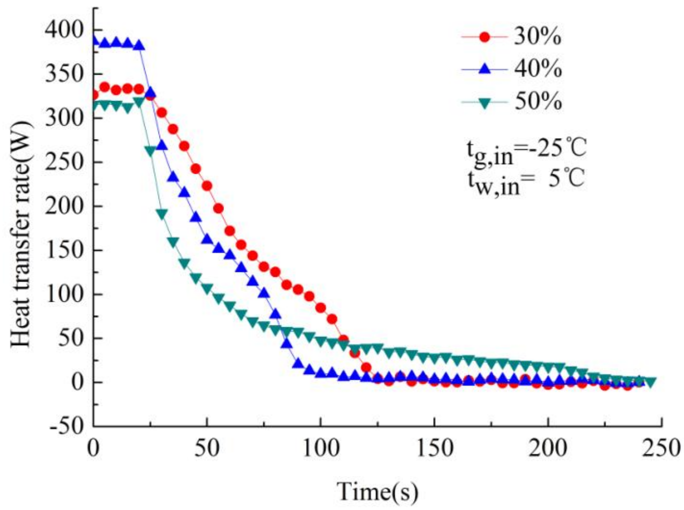

Fig. 13. Heat transfer rates for different fill ratios versus time in the stopping procedure.

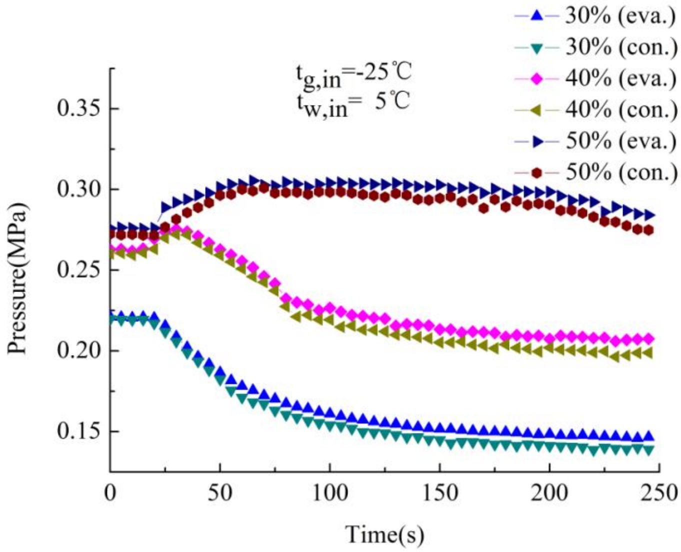

Fig. 14. Pressures for different fill ratios versus time in the stopping procedure.

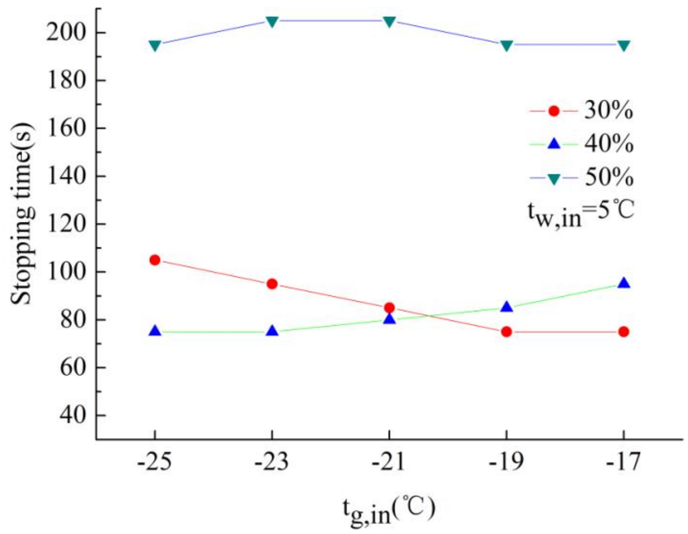

Fig. 15. Variations in stopping time with fill ratio and $t_{g,in.}$.

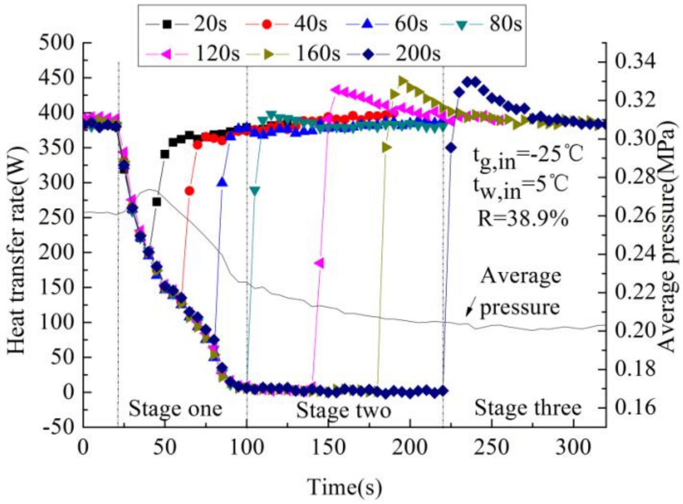

Fig. 16. Rapid restarting performance versus interval time.

Table 1. Geometrical parameters for CSHP.

Component	Inner diameter (mm)	Outer diameter (mm)	Length (mm)
Vapor line	10	12	1300
Liquid line	10	12	1500
Evaporator	25	23	1340
Shell of evaporator	10	12	1340
Condenser	25	23	1340
Shell of condenser	10	12	1340
Helical heat exchanger	147.5	172.5	1340

Table 2. List of experimental testing and monitoring devices.

Device	Specification	Accuracy
Pressure sensor	JT-131	0.5%
Thermocouple	Type T	±0.5°C
Flowmeter	Glass rotameter	2.5%
Scale	Electronic	±0.5g
Data acquisition unit	Agilent 34970	/

Table 3. Comparisons of the calculations and experimental fitting results.

$t_{g,in}$ (°C)		-17	-19	-21	-23	-25
Optimal fill ratio (%)		34.7	34.7	36.8	38.9	38.9
Optimal heat transfer capability (W)	Experimental	314.7	334.7	349.9	366.3	384.6
	calculated	283.4	309.2	335.0	360.7	386.5
	Error	0.099	0.076	0.042	0.015	-0.005
Optimal working temperature (°C)	Experimental	-1.55	-2.05	-3.15	-4.45	-5.15
	calculated	-3.25	-4.05	-4.75	-5.55	-6.25
	Error	0.077	0.083	0.062	0.039	0.037

Table 4. Comparisons of the stopping time for different fill ratios.

Heat transfer	30%	40%	50%
Decreasing to 10% (s)	95	70	125
Decreasing to 5% (s)	105	80	190